Cell Reports

Report

Exonuclease Domain-Containing 1 Enhances MIWI2 piRNA Biogenesis via Its Interaction with TDRD12

Graphical Abstract

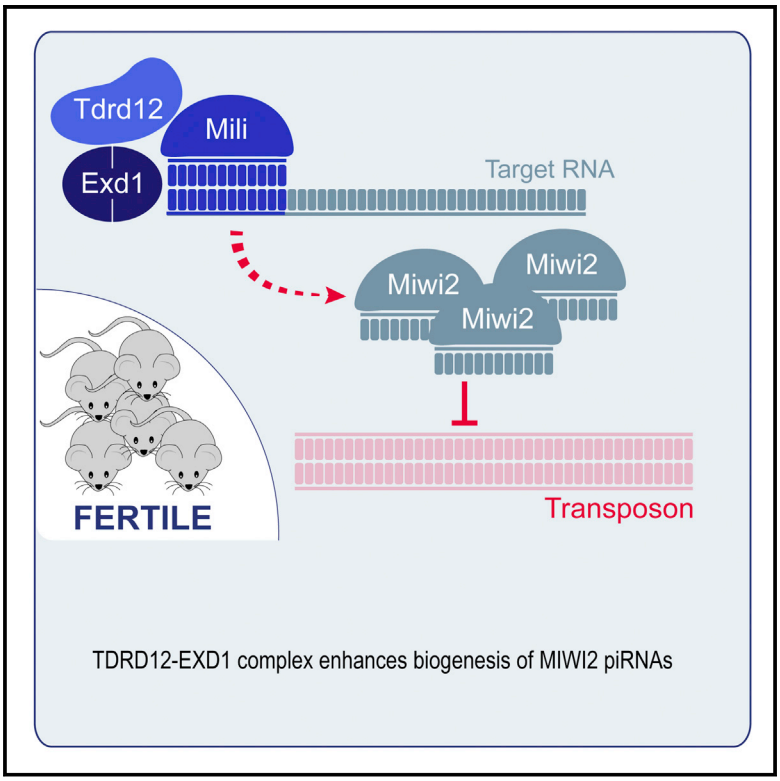

Highlights

- Phased piRNA biogenesis is reduced in *Exd1* mutant mice
- Reduced levels of piRNAs leads to LINE1 de-repression
- EXD1 activity enhances loading of nuclear MIWI2 with piRNAs
- *Exd1* is essential for male fertility in the *Tdrd12*$^{+/-}$ genetic background

Authors

Radha Raman Pandey, David Homolka, Opeyemi Olotu, Ravi Sachidanandam, Noora Kotaja, Ramesh S. Pillai

Correspondence

raman.pandey@unige.ch (R.R.P.), ramesh.pillai@unige.ch (R.S.P.)

In Brief

Pandey et al. demonstrate that EXD1 functionally partners with TDRD12 in the biogenesis of nuclear piRNAs, which is essential for transposon suppression and fertility in mice.

Pandey et al., 2018, Cell Reports *24*, 3423–3432
September 25, 2018
https://doi.org/10.1016/j.celrep.2018.08.087

CellPress

Cell Reports
Report

Exonuclease Domain-Containing 1 Enhances MIWI2 piRNA Biogenesis via Its Interaction with TDRD12

Radha Raman Pandey,[1,4,*] David Homolka,[1,4] Opeyemi Olotu,[2] Ravi Sachidanandam,[3] Noora Kotaja,[2] and Ramesh S. Pillai[1,5,*]

[1]Department of Molecular Biology, University of Geneva, 30 Quai Ernest-Ansermet, 1211 Geneva 4, Switzerland
[2]Institute of Biomedicine, Research Centre for Integrative Physiology and Pharmacology, University of Turku, Turku, Finland
[3]Department of Oncological Sciences, Icahn School of Medicine at Sinai, One Gustave L. Levy Place, New York, NY 10029, USA
[4]These authors contributed equally
[5]Lead Contact
*Correspondence: raman.pandey@unige.ch (R.R.P.), ramesh.pillai@unige.ch (R.S.P.)
https://doi.org/10.1016/j.celrep.2018.08.087

SUMMARY

PIWI proteins and their associated small RNAs, called PIWI-interacting RNAs (piRNAs), restrict transposon activity in animal gonads to ensure fertility. Distinct biogenesis pathways load piRNAs into the PIWI proteins MILI and MIWI2 in the mouse male embryonic germline. While most MILI piRNAs are derived via a slicer-independent pathway, MILI slicing loads MIWI2 with a series of phased piRNAs. Tudor domain-containing 12 (TDRD12) and its interaction partner Exonuclease domain-containing 1 (EXD1) are required for loading MIWI2, but only *Tdrd12* is essential for fertility, leaving us with no explanation for the physiological role of *Exd1*. Using an artificial piRNA precursor, we demonstrate that MILI-triggered piRNA biogenesis is greatly reduced in the *Exd1* mutant. The situation deteriorates in the sensitized *Exd1* mutant (*Exd1*$^{-/-}$;*Tdrd12*$^{+/-}$), where diminished MIWI2 piRNA levels de-repress LINE1 retrotransposons, leading to infertility. Thus, EXD1 enhances MIWI2 piRNA biogenesis via a functional interaction with TDRD12.

INTRODUCTION

Transposons constitute a large part of eukaryotic genomes. While most are defunct sequence fragments, a few functional copies are able to move around in the genome. Transposon mobility is potentially damaging to genome integrity, as it can lead to insertional mutagenesis and deletions (Kazazian, 2004). PIWI proteins and their associated PIWI-interacting RNAs (piRNAs) form a small RNA silencing pathway that is essential for the control of transposable elements in animal gonads (Luteijn and Ketting, 2013). The piRNA pathway in the mouse system is composed of three PIWI members: cytoplasmic MILI and MIWI and nuclear MIWI2 (Pillai and Chuma, 2012). While MIWI and MILI are small RNA-guided endonucleases (slicers) that can destroy RNA targets (De Fazio et al., 2011; Reuter et al., 2011), MIWI2 functions in the nucleus by recruiting a transcriptional silencing machinery to mediate DNA and/or histone methylation of target transposon loci (Aravin et al., 2008; Kojima-Kita et al., 2016).

The male embryonic germline co-expresses MILI and MIWI2, and they serve as a model for understanding mouse piRNA biogenesis. Genetic dissection experiments reveal that two distinct biogenesis mechanisms load these PIWI proteins with their respective piRNAs. A slicer-independent primary processing pathway generates most of the piRNAs associating with MILI (De Fazio et al., 2011), while a MILI slicer-dependent secondary processing pathway creates MIWI2 piRNAs (Aravin et al., 2008; De Fazio et al., 2011; Kuramochi-Miyagawa et al., 2008). Slicing of a target RNA by MILI initiates phased/non-overlapping piRNA production that loads MIWI2 and, to a smaller extent, MILI itself (Yang et al., 2016). Given the obvious need to distinguish itself from PIWI slicing-dependent target RNA degradation, a number of factors are specifically required for the biogenesis of MIWI2 piRNAs (Pillai and Chuma, 2012). These include Tudor domain-containing 1 (TDRD1) (Reuter et al., 2009), MVH (Kuramochi-Miyagawa et al., 2010), TDRD12 (Pandey et al., 2013), FKBP6 (Xiol et al., 2012), GTSF1 (Yoshimura et al., 2018), and exonuclease domain-containing 1 (EXD1) (Yang et al., 2016). With the exception of *Exd1*, loss of all these factors results in unloaded MIWI2 being retained in the cytoplasm. This prevents nuclear repression of transposons, and eventually leads to a male-specific infertility.

EXD1 is an interaction partner of TDRD12 in both mouse testes and the *Bombyx mori* (Silkworm) ovarian cell line BmN4 (Yang et al., 2016). Loss of *Exd1* has a mild effect, as MIWI2 piRNA levels are only reduced and mutant mice are fertile. Here, we demonstrate that *Exd1* becomes essential for male fertility in the *Tdrd12*$^{+/-}$ genetic background. Such sensitized *Exd1* mutants (*Exd1*$^{-/-}$; *Tdrd12*$^{+/-}$) display not only a dramatic reduction in MIWI2 piRNAs but also massive de-repression of LINE1 elements, which leads to an arrest in spermatogenesis. Our results firmly place the TDRD12-EXD1 complex as an essential component of the secondary piRNA biogenesis machinery, with EXD1 enhancing MIWI2 piRNA production.

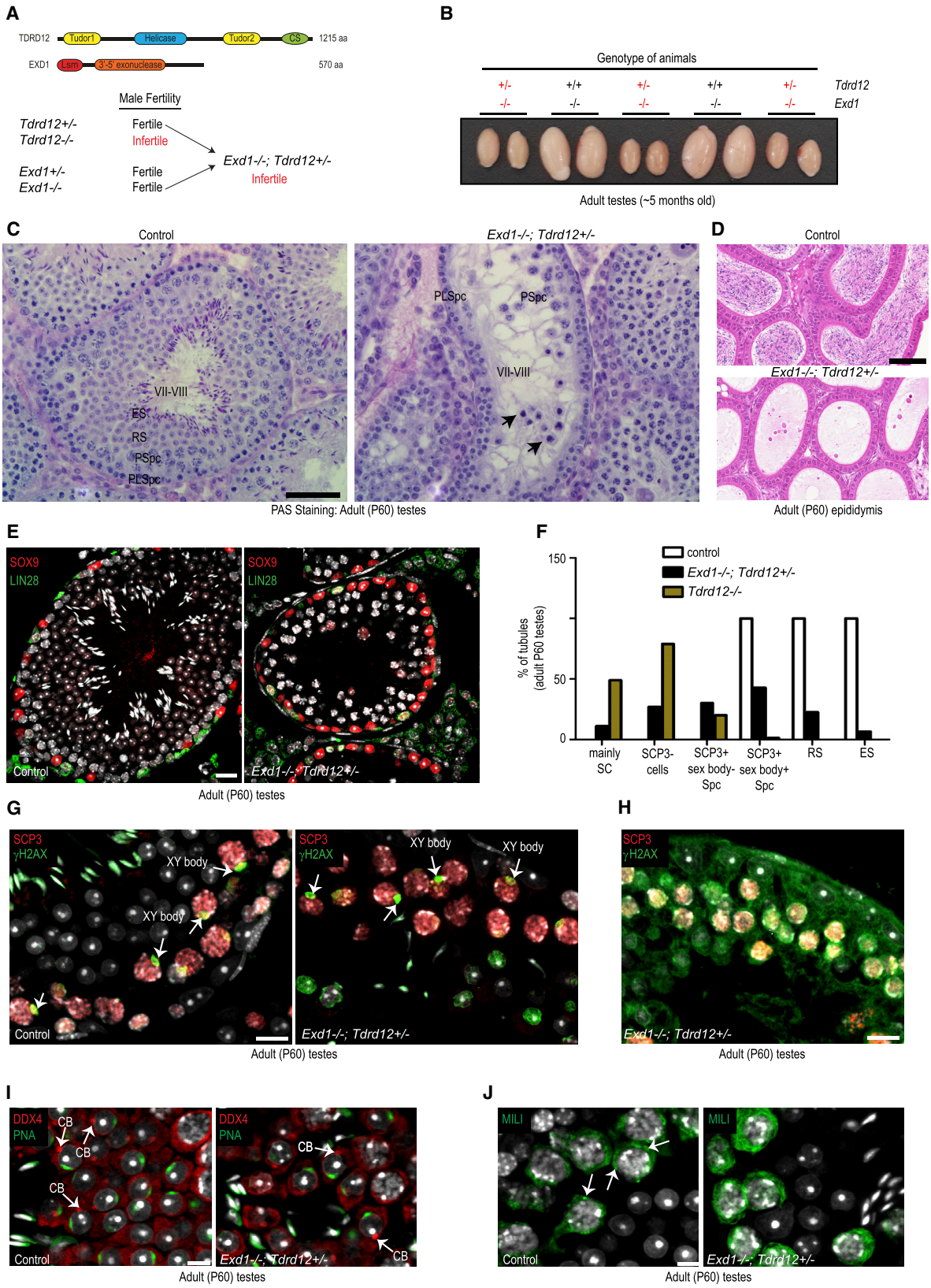

(legend on next page)

RESULTS

MILI Slicing-Triggered Phased piRNA Biogenesis Is Active in the *Exd1* Mutant

We previously reported a mouse model that expresses an artificial piRNA precursor where phased piRNA biogenesis is initiated by MILI slicing, and the generated piRNAs are loaded into both MILI and MIWI2 (Yang et al., 2016). We confirmed that piRNA biogenesis from this precursor is dependent on the ATPase activity of Mouse Vasa Homolog (MVH), one of the secondary processing factors (Wenda et al., 2017). In this study, we examined the requirement of EXD1 for artificial precursor processing (Figure S1; Table S1). MILI slicing initiates phased piRNA biogenesis in the control animals and in the *Exd1* knockout mutant (*Exd1*$^{-/-}$), with the piRNAs accumulating in both MIWI2 and MILI. Consistently, the 16-mer by-product (Wenda et al., 2017) generated by slicing activity is also detected in the *Exd1* mutant (Figure S1). We conclude that, although MIWI2 piRNA levels are globally reduced (Yang et al., 2016), slicer-triggered phased piRNA biogenesis is active in the absence of *Exd1*.

Exd1 Is Essential for Male Fertility in the *Tdrd12*$^{+/-}$ Genetic Background

Given the biochemical interaction between TDRD12 and EXD1 (Yang et al., 2016), we probed the existence of a genetic interaction between them by crossing the fertile homozygous *Exd1*$^{-/-}$ and heterozygous *Tdrd12*$^{+/-}$ animals (see STAR Methods) (Figure 1A). To our surprise, combination of the two fertile genotypes created an infertile mutant, *Exd1*$^{-/-}$; *Tdrd12*$^{+/-}$ (hereinafter referred to as sensitized *Exd1* mutant), indicating a functional interaction between them.

Testes in the adult (~5 months old) sensitized *Exd1* mutants are severely atrophied (Figure 1B). Histological examination indicates disrupted spermatogenesis with a complex phenotype, where spermatogenesis is arrested non-uniformly at different stages of germ cell differentiation. Many tubules contain only somatic Sertoli cells and early spermatogenic cells (spermatogonia and early sepermatocytes) (Figure 1C). On the other hand, other tubule cross-sections show that spermatogenesis has progressed further to pachytene spermatocyte or the round spermatid stage (Figure S1E), and sometimes even elongating spermatids are present (Figure S1F). The dramatic spermatogenic failure was reflected in the complete absence of mature spermatozoa in the cauda epididymis of the sensitized *Exd1* mutant mice (Figure 1D).

To delineate the arrest, we examined the expression of various molecular markers. Sertoli cells (anti-SOX9) and undifferentiated spermatogonia (anti-LIN-28) were normally present in the sensitized *Exd1* mutant seminiferous epithelium (Figure 1E). Examination of testis sections reveal that germ cell development in approximately 27% of the tubules in the adult sensitized *Exd1* mutant was arrested at early meiosis, as shown by the lack of synaptonemal complex (anti-SCP3) and sex body (anti-γH2AX) staining that are hallmarks of pachytene spermatocytes (Figure 1F). The rest of the tubules had progressed further and contained SCP3-positive cells (Figures 1F–1H). Altogether, 30% of the tubules contained SCP3-positive cells that did not have sex bodies, and 43% of the tubules contained both SCP3-positive and sex body-positive cells. The sex body-negative cells mostly represent leptotene and zygotene spermatocytes that already express SCP3 but whose sex bodies have not been assembled yet (Figure 1H). A further 23% of the tubules contained round spermatids as detected by acrosomal staining (peanut agglutinin [PNA]), and only a small fraction of the tubules (7%) contained elongating spermatids (Figures 1F and 1I). This non-uniform arrest in the sensitized *Exd1* mutant is in contrast to the more uniform early spermatocyte arrest seen in the homozygous *Tdrd12*$^{-/-}$ mice (Figures 1F and S1G) (Pandey et al., 2013).

Within the tubules of the sensitized *Exd1* mutant that made it to the post-meiotic round spermatid stage, the acrosomal development appears unaffected (Figures 1F, S2A, and S2B). The PIWI proteins MILI and MIWI were expressed, and they were correctly localized to the chromatoid body (CB) in round spermatids (Figures S2C and S2D). Furthermore, the CB localization of MVH or DDX4 was not affected (Figures S2A and S2B). Interestingly, the localization pattern of MILI in the cytoplasm of mutant pachytene spermatocytes is disrupted, with a more diffuse, thread-like pattern, which is unlike the granular structures that correspond to the intermitochondrial cement (IMC) in the control

Figure 1. *Exd1* Is Conditionally Essential for Male Fertility in Mice

(A) Cartoon showing domain architecture of mouse TDRD12 and EXD1. Summary of phenotypes of various genotypes.

(B) Atrophied testes in the *Exd1*$^{-/-}$; *Tdrd12*$^{+/-}$ (sensitized *Exd1* mutant) animals.

(C) Bouin-fixed paraffin-embedded adult (P60, age in post-natal days) testis sections were stained with PAS stain. Scale bar, 50 μm. Images represent tubule cross-sections at stages VII–VIII of the seminiferous epithelial cycle. Spermatogenesis is severely disrupted in *Exd1*$^{-/-}$; *Tdrd12*$^{+/-}$ mice. Black arrows indicate degenerating cells. See also Figures S1E and S1F.

(D) Paraformaldehyde (PFA)-fixed paraffin-embedded adult cauda epididymides were stained with H&E. Scale bar, 50 μm.

(E) Immunofluorescence staining of PFA-fixed testis sections. Scale bar, 20 μm.

(F) Quantification of tubules containing cell types at specific phase of differentiation in testes of animals with indicated genotypes. Presented as percentage of tubules at specific phases among all tubules in the testis cross-section.

(G) Immunofluorescence staining. γH2AX-positive sex bodies (XY body) in pachytene spermatocytes are indicated by white arrows. Scale bar, 10 μm.

(H) SCP3-positive but sex body-negative early spermatocytes. Scale bar, 10 μm.

(I) Immunofluorescence staining using anti-DDX4 (red), combined with acrosomal staining with PNA-lectin (green). Some DDX4-positive CBs are indicated with white arrows. Scale bar, 10 μm.

(J) Immunofluorescence staining showing altered distribution of MILI in *Exd1*$^{-/-}$; *Tdrd12*$^{+/-}$ spermatocytes. The arrows indicate a normal granular pattern in the control testes. Scale bar, 10 μm. See also Figures S2C and S2D.

In all fluorescent images, DAPI (gray) stains nuclei. PLSpc, preleptotene spermatocytes; PSpc, pachytene spermatocytes; RS, round spermatids; ES, condensed elongating spermatids; SC, Sertoli cell; Spc, spermatocyte.

See also Figures S1 and S2.

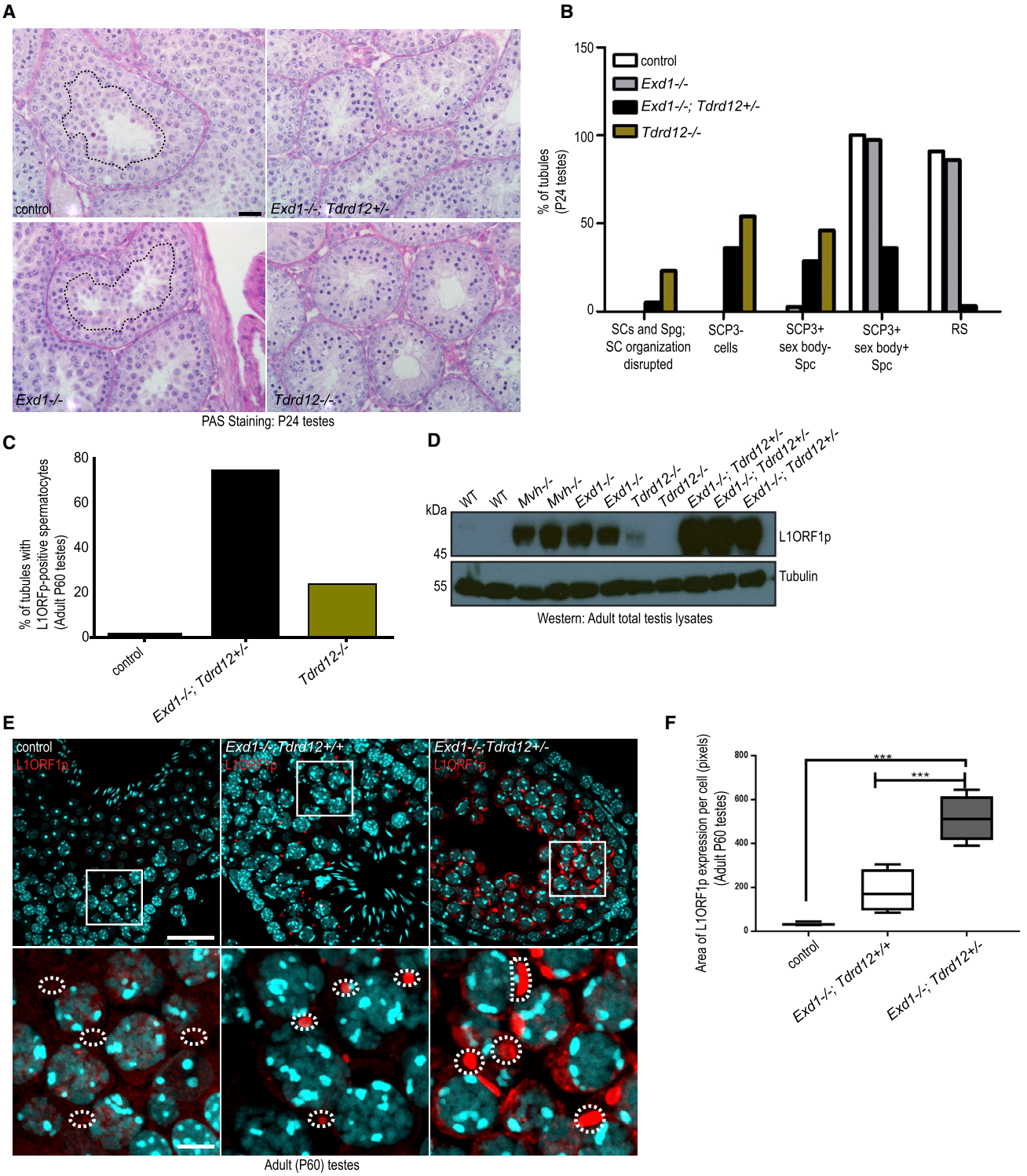

Figure 2. Early Spermatogenic Arrest and Transposon De-repression in the *Exd1*$^{-/-}$;*Tdrd12*$^{+/-}$ Mutant

(A) Bouin-fixed paraffin-embedded P24 (age in days after birth) testis sections were stained with PAS. Black dashed lines indicate a border between meiotic spermatocytes and haploid round spermatids. Scale bar, 20 μm.

(B) Quantification of tubules containing cell types at specific phase of differentiation. SC, Sertoli cell; Spg, spermatogonium; Spc, spermatocyte; RS, round spermatid.

(legend continued on next page)

testes (Figure 1J). Taken together, although loss of *Exd1* alone is tolerated, a concomitant reduction in *Tdrd12* gene dosage (as in the *Tdrd12*$^{+/-}$ background) results in male-specific infertility, which is a characteristic piRNA pathway mutant phenotype.

Early Spermatogenic Arrest Is Accompanied by De-repression of Transposons

Given the mixed spermatogenic arrest phenotype in the adult mutant, we wanted to determine whether the block already sets in during the first wave of spermatogenesis in juvenile testis. To this end, we examined the first wave of spermatogenesis in juvenile testis. Control post-natal day (P)24 testes contained haploid round spermatids at steps 1–7 of differentiation, as evaluated on the basis of acrosomal staining (Figures 2A and S1G). As reported earlier (Yang et al., 2016), the deletion of *Exd1* has no obvious effects on progression of spermatogenesis, and *Exd1* mutant P24 testes contained tubules with round spermatids (Figures 2A and S1G). In contrast, one third of the tubules in the sensitized *Exd1* mutant P24 testes did not reach the pachytene spermatocyte phase, as evaluated by the lack of SCP3-positive cells in the tubules (Figure 2B), and only a third of the tubules contained SCP3 and sex body-positive pachytene spermatocytes (Figure 2B). Haploid round spermatids positive for acrosomal staining or the MILI/MIWI-containing CBs were very few in the P24 sensitized *Exd1* mutant testes (Figure 2B). In comparison, spermatogenesis in the *Tdrd12*$^{-/-}$ mutant was more severely disrupted, with an absence of SCP3- and sex body-positive pachytene spermatocytes (Figure 2B). Indeed, 23% of the *Tdrd12*$^{-/-}$ tubules contained only spermatogonia and Sertoli cells (Figure 2B), and the organization of the epithelium in these tubules was disrupted with Sertoli cell nuclei forming a layer on the luminal side of spermatogonia.

Given the role of TDRD12 and EXD1 in the piRNA pathway, we examined whether the infertility in the sensitized *Exd1* mutant is linked to de-repression of transposons. De-repression of LINE1 (L1) retrotransposons is already reported for the individual knockout mutants of *Tdrd12*$^{-/-}$ and *Exd1*$^{-/-}$ (Pandey et al., 2013; Yang et al., 2016). We stained adult testis sections with antibodies to L1ORF1p, a protein expressed from active endogenous L1 elements. Confirming a strong expression of the transposon elements, ~75% of the tubules in the sensitized *Exd1* mutant were positive for L1ORF1p expression (Figure 2C). Only 24% of tubules in the *Tdrd12*$^{-/-}$ testes were positive for LINE1, partly because of the early meiotic arrest and loss of germ cells by apoptosis. This dramatic de-repression of L1 elements is revealed when we compared L1ORF1p protein levels in adult (P60) testis lysates across different genotypes. In biological triplicates of the sensitized *Exd1* mutant, we observed a striking accumulation of the transposon-expressed protein, at a level much higher than that seen in the *Exd1*$^{-/-}$ testes (Figure 2D). Immunofluorescence analysis reveals that the L1ORF1p protein accumulates in the cytoplasm of pachytene spermatocytes in the *Exd1* mutant, mostly in a single granule (Figures 2E and 2F). This is accentuated in the sensitized *Exd1* mutant testes, where the massively expressed L1ORF1p protein accumulates in a larger granule (Figures 2E and 2F). These analyses reveal that, despite having late post-meiotic spermatogenic cells in some tubules of the sensitized *Exd1* mutant testes, most defects in spermatogenesis occur early and display a concomitant L1 retrotransposon de-repression.

Reduced Levels of piRNAs in the Sensitized *Exd1*$^{-/-}$ Mutant

Given the transposon de-repression in the sensitized *Exd1* mutant, we examined the status of small RNAs. We prepared deep sequencing libraries (in biological triplicates) of total small RNAs (20–40 nt) isolated from neonatal (P0) testes (Figure S3A). The following two genotypes were compared: fertile *Exd1*$^{+/-}$; *Tdrd12*$^{+/-}$ and the infertile sensitized mutant *Exd1*$^{-/-}$; *Tdrd12*$^{+/-}$. Read-length distribution of multi-mappers shows a minor peak of potential piRNA-sized reads at 26–28 nt in both libraries and an additional abundant peak of 30- to 34-nt reads present only in the sensitized mutant (Figures 3A and 3B). Analysis of genome annotations indicates that the majority of the piRNAs map to repeats in both sense (Figures S3C and S3D) and antisense orientations, and, strikingly, the sensitized *Exd1* mutant showed a dramatic 2.5-fold decrease in antisense repeat sequences (Figure 3C). Sequences mapping to non-LTR retrotransposons, like LINE (L1) and SINE, and to LTR retrotransposons are largely deceased in the sensitized mutant compared to the control libraries (Figure 3D). When examined at the level of individual transposons, most of the highly expressed sense and antisense piRNAs targeting LINE, SINE, and LTR elements are decreased (Figures 3E and S3D). This is further evident by plotting distributions along the L1 consensus sequence, which reveals a drastic drop in mainly antisense piRNAs in the sensitized mutant compared to the control (Figures 3F and 3G).

To understand whether the reduced piRNA levels might explain the infertility in the sensitized mutant, we compared it to the previously published dataset from the *Exd1*$^{-/-}$ knockout mutant and control *Exd1*$^{+/-}$ animals, both of which are fertile. As previously reported (Yang et al., 2016), the *Exd1*$^{-/-}$ mutant has reduced antisense piRNAs when compared to the *Exd1*$^{+/-}$ control animals (Figure 3F). To our surprise, this overall decrease is similar in the fertile *Exd1*$^{-/-}$ mutant and the infertile sensitized *Exd1* mutant (*Tdrd12*$^{+/-}$; *Exd1*$^{-/-}$) (Figures 3F and 3G). Next, we examined piRNA sequence signatures of MILI slicing, as this initiates the phased piRNA biogenesis that loads MIWI2

(C) PFA-fixed paraffin-embedded testis sections were immunostained with anti-LIORF1p antibodies. Quantification of tubules containing LIORF1p-positive spermatocytes, presented as percentage of positive tubules among all tubules in the testis cross-section.
(D) Western analysis of L1ORF1p with adult (P60) testes lysates (biological replicates tested).
(E) PFA-fixed paraffin-embedded testis sections were immunostained with anti-LIORF1p antibodies (red). Some cytoplasmic accumulations of LIORF1p in pachytene spermatocytes (PSpc) are indicated with dotted circles. Scale bars, 20 μm.
(F) Quantification of the L1ORF1p signal inside the circled areas in (E) to get an estimation of the size of L1ORF1p-positive granules. Error bars refer to SD between the granules in different cells. Asterisk (*) indicates significant difference.
See also Figure S1G.

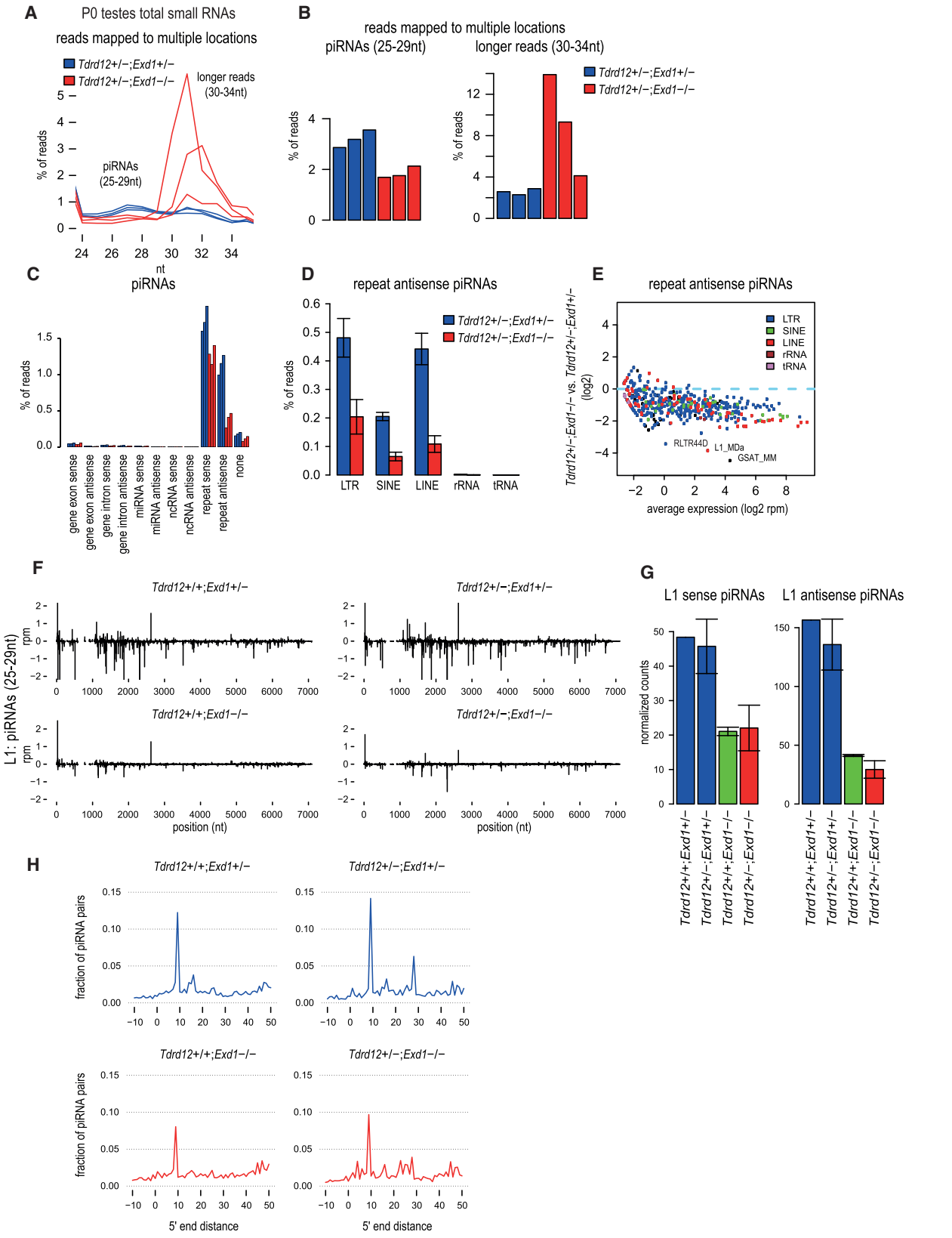

(legend on next page)

(Yang et al., 2016). The first small RNA (secondary piRNA) in this series has its 5′ end generated by MILI. This results in a sequence feature called the Ping-pong signature (10-nt overlap of 5′ ends of piRNAs with opposite orientation), which is reduced in the *Exd1*$^{-/-}$ and the sensitized *Exd1* mutants (Figure 3H), indicating an impairment of MILI slicing-triggered piRNA biogenesis. Nevertheless, the overall fraction of piRNA pairs displaying biogenesis via MILI slicing is similar in both the fertile *Exd1* and infertile sensitized *Exd1* mutants. We conclude that loss of *Exd1* results in reduction of antisense piRNAs and transposon activation, but whether fertility is affected depends on the status of the *Tdrd12* allele.

Reduced Loading of MIWI2 with piRNAs in the Sensitized *Exd1* Mutant

Since both MILI and MIWI2 contribute to the embryonic or perinatal piRNA pool, we directly examined piRNAs associated with the two proteins. We carried out immunoprecipitations (in biological duplicates) from P0 testes, followed by 5′ end-labeling (Figure 4A). The following genotypes were used: fertile *Exd1*$^{+/-}$ and *Exd1*$^{-/-}$ and the infertile sensitized *Exd1* mutant. While the overall levels of MILI-loaded piRNAs are unaffected in all the genotypes, a clear impact on biogenesis of MIWI2 piRNAs is noted. Compared to the control *Exd1*$^{+/-}$, the levels of MIWI2 piRNAs are dramatically reduced in both the fertile *Exd1*$^{-/-}$ mutant and the infertile sensitized *Exd1* mutant (Figure 4A).

Deep sequencing analysis (Figures 4B and S4) reveals that, among the remaining MIWI2 piRNAs, the antisense repeat piRNAs mapping to LINE elements are mainly affected in the *Exd1* and sensitized *Exd1* mutant (Figure 4C). Larger reduction is observed in the sensitized *Exd1* mutant when compared to the *Exd1* mutant (Figure 4D). This is also reflected in decreased mapping of reads along the length of the L1 consensus sequence (Figure 4E). Levels of antisense repeat reads in MILI complexes were largely unaffected (Figures S4C and S4D). All this indicates that loss of *Exd1* in the *Tdrd12*$^{+/-}$ genetic background has a profound impact on MIWI2 piRNA biogenesis.

Abundant Levels of tRNA Fragments in the Mutant Small RNA Libraries

We turned our attention to the 30- to 34-nt reads abundantly present in the sensitized *Exd1* mutant P0 testes (Figures 3A and 3B). Such sequences essentially originate from the sense strand of repetitive elements in the genome (Figure S3E) and are identified as mapping almost exclusively to tRNAs (Figure S3F). When examined for individual tRNAs, the 30- to 34-nt reads originating from at least 30 different tRNAs are increased in the sensitized mutant (Figures S3G and S3H). Mapping of these reads to tRNA sequences reveals that they share the same 5′ ends as the mature tRNAs, while the 3′ ends lie 30–34 nt downstream within the tRNA sequence (Figure S3I). Mapping the 3′ ends on the tRNA secondary structure sequence reveals that these 5′ tRNA fragments are generated by cleavages around the start of the anticodon loop (Figure S3J). Examination of the 25- to 29-nt piRNA sequences shows that representation of tRNA-originating reads are very low in both the fertile *Exd1*$^{+/-}$; *Tdrd12*$^{+/-}$ control and infertile sensitized *Exd1* mutant total small RNA libraries (Figure S3H). Also, the tRNA fragments did not reveal a pronounced U1 bias that is typical of piRNAs. Finally, they are also not enriched in the MILI or MIWI2 complexes (Figure 4B). Taken together, we conclude that the sensitized *Exd1* mutant accumulates longer reads that are 5′ tRNA fragments, but these do not enter the PIWI complexes.

DISCUSSION

The piRNA biogenesis pathway performs two key functions. First, it extracts genetic information stored in piRNA clusters that are equivalent to sequence archives containing fragments of all transposons present within a genome (primary processing). This is critical in environments like the mouse embryonic germline where the initial pool of piRNAs has to be created *de novo*, without assistance from pre-existing (or inherited) piRNAs. Second, it sources new piRNAs from targets of piRNAs in an adaptive response pathway (secondary processing). The latter mechanism is critical for genome defense, as new precursors are channeled into the biogenesis machinery. It also allows selective amplification of a particular set of piRNA sequences defined by the target sequence. Parallels can be seen in the *Drosophila* ovarian system where a slicer-dependent phased piRNA production (secondary processing) operates in the germline compartment (Han et al., 2015; Homolka et al., 2015; Mohn et al., 2015). In contrast, a slicer-independent primary processing mechanism is active in the fly soma (Darricarrère et al.,

Figure 3. Sensitized *Exd1*$^{-/-}$ Mutant *Exd1*$^{-/-}$;*Tdrd12*$^{+/-}$ Displays Reduced Levels of piRNAs

(A) Comparison of read length distribution of small RNAs isolated from testes of P0 of indicated genotypes (triplicate biological replicates). Only reads from repetitive regions mapped to multiple locations are plotted. While the piRNA reads (25–29 nt) are depleted in *Tdrd12*$^{+/-}$;*Exd1*$^{-/-}$, there is an increase of longer reads (30–34 nt).

(B) Comparison of the amount of reads corresponding to piRNAs and the 30- to 34-nt reads in individual samples.

(C) Classification of piRNA reads shows that mainly repeat antisense reads are affected in *Tdrd12*$^{+/-}$;*Exd*$^{-/-}$.

(D) Classification of repeat antisense piRNAs based on repeat class. Error bars refer to SD between the replicas.

(E) The MA plot compares the levels of piRNAs targeting individual repeats. Individual repeat families are indicated in different colors. Absence of EXD1 results in overall decrease in the repeat antisense piRNAs.

(F) Distribution of piRNA 5′ ends along the L1 repeat consensus sequence. While the sense piRNAs are plotted above the horizontal axis, the antisense piRNAs are indicated below the axis. Similar decrease of mainly antisense piRNAs was observed for both *Exd1* mutant (*Tdrd12*$^{+/+}$;*Exd*$^{-/-}$) and sensitized *Exd1* mutant (*Tdrd12*$^{+/-}$;*Exd*$^{-/-}$).

(G) Comparison of piRNA amounts mapped to L1 consensus shows the decreased levels of L1 piRNAs in the *Tdrd12*$^{+/+}$;*Exd1*$^{-/-}$ and *Tdrd12*$^{+/-}$;*Exd1*$^{-/-}$. Error bars refer to SD between the replicas. There was only one replica for *Tdrd12*$^{+/+}$;*Exd1*$^{+/-}$.

(H) Plots show the preferred 5′ end distances between the targeting and produced piRNAs for L1 transposon. The ping-pong signature (corresponding to peak at distance 9) is decreased when the EXD1 is absent.

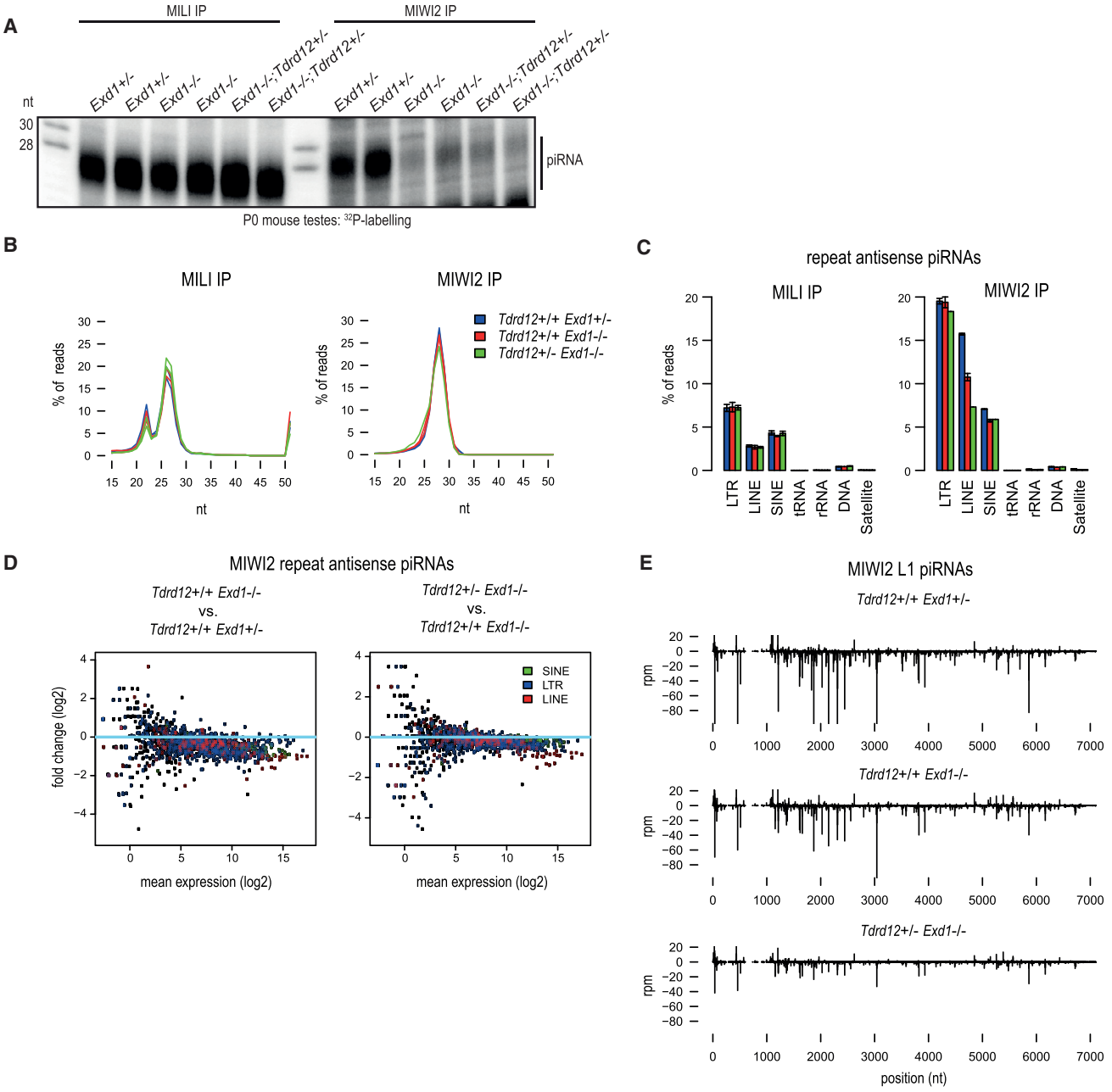

Figure 4. Lack of EXD1 Results in Reduced Levels of MIWI2 piRNAs

(A) Small RNAs associated with MILI or MIWI2 were immunopurified from P0 mouse testes. 5′ end-labeling shows almost complete lack of MIWI2-associated piRNAs in mutants lacking EXD1.

(B) Comparison of length distribution of MILI- and MIWI2-associated reads.

(C) piRNAs targeting LINE elements are underrepresented in MIWI2 libraries from genotypes lacking EXD1. Error bars refer to SD between the replicas.

(D) MA plots compare the levels of MIWI2 piRNAs targeting individual repeats between specified genotypes. Individual repeat families are shown in different colors. Lack of EXD1 has greater effect on MIWI2 piRNA levels targeting LINE repeats when combined with *Tdrd12*$^{+/-}$ genotype (sensitized *Exd1* mutant).

(E) Distribution of MIWI2 piRNA 5′ ends along the L1 repeat consensus sequence. While the sense piRNAs are plotted above the horizontal axis, the antisense piRNAs are indicated below the axis. The levels of antisense piRNAs are affected in *Exd1* mutant (*Tdrd12*$^{+/+}$;*Exd*$^{-/-}$) and even more so in the sensitized *Exd1* mutant (*Tdrd12*$^{+/-}$;*Exd*$^{-/-}$).

See also Figure S2E.

2013). The presence of specific sequence elements is sufficient to allow entry of a transcript into primary processing in the fly soma (Homolka et al., 2015; Ishizu et al., 2015). Such sequences are believed to serve as recruitment sites for biogenesis factors. Biogenesis of piRNAs is a cytoplasmic event that takes place in perinuclear RNA-protein granules generally termed as nuage (Aravin et al., 2009; Lim and Kai, 2007). In fact, direct tethering of nuage-localizing piRNA pathway factors to a transcript is also sufficient to trigger phased primary processing from artificial reporters in fly ovaries (Pandey et al., 2017; Rogers et al., 2017). Thus, two distinct (slicer-dependent and -independent) pathways identify transcripts as piRNA precursors in mice and flies, but both are expected to direct them into a common biogenesis machinery that results in phased piRNA generation.

The goal of this investigation was to determine the physiological role of the secondary piRNA biogenesis factor EXD1. Using an artificial reporter (Figure S1), we demonstrate that MILI slicing-triggered phased piRNA biogenesis is still active in the *Exd1* mutant mice. However, the overall levels of antisense piRNAs targeting the transposons are lower (Figures 3C–3F). This is mainly due to reduced levels of MIWI2 piRNAs in the *Exd1* mutant (Figure 4A), which is consistent with an earlier observation (Yang et al., 2016). Despite such dramatically reduced levels of MIWI2-bound piRNAs, the *Exd1* mutant mice surprisingly reveal no long-term fertility defects, as the inbred colony has been maintained in our laboratory for over 3 years. Now we find that the additional loss of one *Tdrd12* allele (sensitized *Exd1* mutant) upsets this delicate environment, resulting in male infertility. Significantly, when compared between the two *Exd1* mutants, there is no dramatic difference in overall piRNA levels in total small RNAs or MIWI2- or MILI-bound species (Figures 3F and 4E). Additionally, our examination of total small RNA libraries from P12–P14 animals also did not reveal any dramatic piRNA differences between the two genotypes (Figure S5). Consistent with the reduced piRNA loading, the normally exclusively nuclear MIWI2 shows a nucleo-cytoplasmic distribution in both the *Exd1* (Yang et al., 2016) and the sensitized *Exd1* mutants (Figure S2E). However, sequence analysis shows that MIWI2-bound antisense L1 piRNAs are more reduced in the infertile sensitized *Exd1* mutant when compared to the fertile *Exd1*$^{-/-}$ animals (Figures 4C and 4E). We propose that the altered sequence content might be the reason for the de-repression of L1 elements in the adult sensitized *Exd1* mutant (Figures 2D–2F) and consequent infertility (Figure 1).

We did not observe the presence of tRNA fragments (tRFs) in the total small RNA libraries from the *Exd1* mutant (Yang et al., 2016), but its presence in the sensitized *Exd1* mutant may be a consequence of transposon deregulation. A variety of tRNAs can be identified in small RNA libraries (Kumar et al., 2016), and some of the sequences we identified here are identical to the ones already described in testes of mice undergoing stress caused by dietary restriction (Sharma et al., 2016). Many tRFs are described as an outcome of stress conditions (Thompson and Parker, 2009), and it is likely that the loss of piRNA pathway factors and consequent transposon de-repression might provoke similar situations. Although it is possible that some of the phenotypic outcomes in the sensitized *Exd1* mutant are caused by the tRFs, we currently have no evidence to suggest a direct effect, especially given that we did not find similar tRFs in the P12–P14 libraries (Figure S5). Overall, our study points to a role for EXD1 as an enhancer of the secondary piRNA biogenesis pathway, acting in collaboration with its interaction partner TDRD12, to suppress transposable elements in the mammalian male germline.

STAR★METHODS

Detailed methods are provided in the online version of this paper and include the following:

- KEY RESOURCES TABLE
- CONTACT FOR REAGENT AND RESOURCE SHARING
- EXPERIMENTAL MODEL AND SUBJECT DETAILS
  - Animal Work
  - Exd1 and Tdrd12 mutant mice
- METHOD DETAILS
  - Histology
  - Preparation of tissue samples for immunostaining
  - Immunofluorescence analysis
  - Imaging
  - Antibodies
- QUANTIFICATION AND STATISTICAL ANALYSIS
  - Analysis of reads originating from artificial piRNA precursor (Rosa26-pi)
  - Analysis of total small RNA libraries
  - Analysis of small RNA libraries from MILI and MIWI2 complexes
- DATA AND SOFTWARE AVAILABILITY

SUPPLEMENTAL INFORMATION

Supplemental Information includes five figures and one table and can be found with this article online at https://doi.org/10.1016/j.celrep.2018.08.087.

ACKNOWLEDGMENTS

We thank the EMBL Genomics core facility for sequencing services. This work was supported by grants to R.S.P. from the Swiss National Science Foundation: an ERC transfer grant (GermMethylation), an Origin-of-Pi project grant, and funding from the NCCR RNA & Disease Network. The Kotaja lab is supported by the research grants from the Academy of Finland and the Sigrid Jusélius Foundation. Work in the Pillai lab is supported by the Republic and Canton of Geneva.

AUTHOR CONTRIBUTIONS

R.R.P. initiated the study with mouse crosses and performed biochemical experiments; O.O. performed spermatogenesis analysis, with guidance from N.K.; D.H. performed computational analyses, with help from R.S.; R.R.P. and R.S.P. performed coordination and manuscript preparation, with input from others.

DECLARATION OF INTERESTS

The authors declare no competing interests.

Received: January 18, 2018
Revised: August 6, 2018
Accepted: August 29, 2018
Published: September 25, 2018

REFERENCES

Aravin, A.A., Sachidanandam, R., Bourc'his, D., Schaefer, C., Pezic, D., Toth, K.F., Bestor, T., and Hannon, G.J. (2008). A piRNA pathway primed by individual transposons is linked to de novo DNA methylation in mice. Mol. Cell *31*, 785–799.

Aravin, A.A., van der Heijden, G.W., Castañeda, J., Vagin, V.V., Hannon, G.J., and Bortvin, A. (2009). Cytoplasmic compartmentalization of the fetal piRNA pathway in mice. PLoS Genet. *5*, e1000764.

Darricarrère, N., Liu, N., Watanabe, T., and Lin, H. (2013). Function of Piwi, a nuclear Piwi/Argonaute protein, is independent of its slicer activity. Proc. Natl. Acad. Sci. USA *110*, 1297–1302.

De Fazio, S., Bartonicek, N., Di Giacomo, M., Abreu-Goodger, C., Sankar, A., Funaya, C., Antony, C., Moreira, P.N., Enright, A.J., and O'Carroll, D. (2011). The endonuclease activity of Mili fuels piRNA amplification that silences LINE1 elements. Nature *480*, 259–263.

Han, B.W., Wang, W., Li, C., Weng, Z., and Zamore, P.D. (2015). Noncoding RNA. piRNA-guided transposon cleavage initiates Zucchini-dependent, phased piRNA production. Science *348*, 817–821.

Homolka, D., Pandey, R.R., Goriaux, C., Brasset, E., Vaury, C., Sachidanandam, R., Fauvarque, M.O., and Pillai, R.S. (2015). PIWI slicing and RNA elements in precursors instruct directional primary piRNA biogenesis. Cell Rep. *12*, 418–428.

Ishizu, H., Iwasaki, Y.W., Hirakata, S., Ozaki, H., Iwasaki, W., Siomi, H., and Siomi, M.C. (2015). Somatic primary piRNA biogenesis driven by *cis*-acting RNA elements and *trans*-acting Yb. Cell Rep. *12*, 429–440.

Kazazian, H.H., Jr. (2004). Mobile elements: drivers of genome evolution. Science *303*, 1626–1632.

Kojima-Kita, K., Kuramochi-Miyagawa, S., Nagamori, I., Ogonuki, N., Ogura, A., Hasuwa, H., Akazawa, T., Inoue, N., and Nakano, T. (2016). MIWI2 as an effector of DNA methylation and gene silencing in embryonic male germ cells. Cell Rep. *16*, 2819–2828.

Kumar, P., Kuscu, C., and Dutta, A. (2016). Biogenesis and function of transfer RNA-related fragments (tRFs). Trends Biochem. Sci. *41*, 679–689.

Kuramochi-Miyagawa, S., Watanabe, T., Gotoh, K., Totoki, Y., Toyoda, A., Ikawa, M., Asada, N., Kojima, K., Yamaguchi, Y., Ijiri, T.W., et al. (2008). DNA methylation of retrotransposon genes is regulated by Piwi family members MILI and MIWI2 in murine fetal testes. Genes Dev. *22*, 908–917.

Kuramochi-Miyagawa, S., Watanabe, T., Gotoh, K., Takamatsu, K., Chuma, S., Kojima-Kita, K., Shiromoto, Y., Asada, N., Toyoda, A., Fujiyama, A., et al. (2010). MVH in piRNA processing and gene silencing of retrotransposons. Genes Dev. *24*, 887–892.

Langmead, B., Trapnell, C., Pop, M., and Salzberg, S.L. (2009). Ultrafast and memory-efficient alignment of short DNA sequences to the human genome. Genome Biol. *10*, R25.

Lim, A.K., and Kai, T. (2007). Unique germ-line organelle, nuage, functions to repress selfish genetic elements in *Drosophila melanogaster*. Proc. Natl. Acad. Sci. USA *104*, 6714–6719.

Luteijn, M.J., and Ketting, R.F. (2013). PIWI-interacting RNAs: from generation to transgenerational epigenetics. Nat. Rev. Genet. *14*, 523–534.

Mohn, F., Handler, D., and Brennecke, J. (2015). Noncoding RNA. piRNA-guided slicing specifies transcripts for Zucchini-dependent, phased piRNA biogenesis. Science *348*, 812–817.

Olson, A.J., Brennecke, J., Aravin, A.A., Hannon, G.J., and Sachidanandam, R. (2008). Analysis of large-scale sequencing of small RNAs. Pac. Symp. Biocomput. *13*, 126–136.

Pandey, R.R., Tokuzawa, Y., Yang, Z., Hayashi, E., Ichisaka, T., Kajita, S., Asano, Y., Kunieda, T., Sachidanandam, R., Chuma, S., et al. (2013). Tudor domain containing 12 (TDRD12) is essential for secondary PIWI interacting RNA biogenesis in mice. Proc. Natl. Acad. Sci. USA *110*, 16492–16497.

Pandey, R.R., Homolka, D., Chen, K.M., Sachidanandam, R., Fauvarque, M.O., and Pillai, R.S. (2017). Recruitment of Armitage and Yb to a transcript triggers its phased processing into primary piRNAs in *Drosophila* ovaries. PLoS Genet. *13*, e1006956.

Pillai, R.S., and Chuma, S. (2012). piRNAs and their involvement in male germline development in mice. Dev. Growth Differ. *54*, 78–92.

R Core Team (2017). R: A Language and Environment for Statistical Computing (Vienna, Austria: R Foundation for Statistical Computing).

Reuter, M., Chuma, S., Tanaka, T., Franz, T., Stark, A., and Pillai, R.S. (2009). Loss of the Mili-interacting Tudor domain-containing protein-1 activates transposons and alters the Mili-associated small RNA profile. Nat. Struct. Mol. Biol. *16*, 639–646.

Reuter, M., Berninger, P., Chuma, S., Shah, H., Hosokawa, M., Funaya, C., Antony, C., Sachidanandam, R., and Pillai, R.S. (2011). Miwi catalysis is required for piRNA amplification-independent LINE1 transposon silencing. Nature *480*, 264–267.

Rogers, A.K., Situ, K., Perkins, E.M., and Toth, K.F. (2017). Zucchini-dependent piRNA processing is triggered by recruitment to the cytoplasmic processing machinery. Genes Dev. *31*, 1858–1869.

Sharma, U., Conine, C.C., Shea, J.M., Boskovic, A., Derr, A.G., Bing, X.Y., Belleannee, C., Kucukural, A., Serra, R.W., Sun, F., et al. (2016). Biogenesis and function of tRNA fragments during sperm maturation and fertilization in mammals. Science *351*, 391–396.

Thompson, D.M., and Parker, R. (2009). Stressing out over tRNA cleavage. Cell *138*, 215–219.

Wenda, J.M., Homolka, D., Yang, Z., Spinelli, P., Sachidanandam, R., Pandey, R.R., and Pillai, R.S. (2017). Distinct roles of RNA helicases MVH and TDRD9 in PIWI slicing-triggered mammalian piRNA biogenesis and function. Dev. Cell *41*, 623–637.e9.

Xiol, J., Cora, E., Koglgruber, R., Chuma, S., Subramanian, S., Hosokawa, M., Reuter, M., Yang, Z., Berninger, P., Palencia, A., et al. (2012). A role for Fkbp6 and the chaperone machinery in piRNA amplification and transposon silencing. Mol. Cell *47*, 970–979.

Yang, Z., Chen, K.M., Pandey, R.R., Homolka, D., Reuter, M., Janeiro, B.K., Sachidanandam, R., Fauvarque, M.O., McCarthy, A.A., and Pillai, R.S. (2016). PIWI slicing and EXD1 drive biogenesis of nuclear piRNAs from cytosolic targets of the mouse piRNA pathway. Mol. Cell *61*, 138–152.

Yoshimura, T., Watanabe, T., Kuramochi-Miyagawa, S., Takemoto, N., Shiromoto, Y., Kudo, A., Kanai-Azuma, M., Tashiro, F., Miyazaki, S., Katanaya, A., et al. (2018). Mouse GTSF1 is an essential factor for secondary piRNA biogenesis. EMBO Rep, Published online February 7, 2018. https://doi.org/10.15252/embr.201642054.

STAR★METHODS

KEY RESOURCES TABLE

REAGENT or RESOURCE	SOURCE	IDENTIFIER
Antibodies		
Mouse monoclonal anti-MILI (13E3)	(Reuter et al., 2009) Millipore	MABE363; RRID: AB_2737284
Rabbit polyclonal anti-MIWI	(Reuter et al., 2011)	N/A
Rabbit polyclonal anti-MIWI2	(Pandey et al., 2013)	N/A
Rabbit polyclonal anti-LINE1 ORF1p	(Wenda et al., 2017)	N/A
Rabbit polyclonal anti-MVH	Abcam	ab13840; RRID:AB_443012
anti-MIWI	Cell signaling	G82; RRID:AB_2165432
anti-SCP3	Santa Cruz	sc-33195; RRID:AB_656732
anti-SOX9	Millipore	AB5535; RRID:AB_2239761
anti γ-H2AX	Millipore	05-636; RRID:AB_309864
anti-MILI/PIWIL-2, clone 13E-3	Millipore	MABE363;RRID:AB_2737284
anti-LIN28	R&D systems	AF3757; RRID:AB_2234537
Rabbit polyclonal anti-β-TUBULIN	Abcam	ab6046; RRID:AB_2210370
Chemicals, Peptides, and Recombinant Proteins		
Sodium deoxycholate	Sigma	30968
Complete EDTA-free protease inhibitor	Roche	11 873 580 001
Tissue-Tek CRYO-OCT Compound	Fisher Scientific	14-373-65
DAPI	Bio-Rad	10043282; RRID:AB_2737285
Bouin's solution	Sigma	HT10132
Hematoxylin solution, Harris modified	Sigma	HHS16
Eosin Y solution with phloxine	Sigma	HT110332
Permount	Fisher Scientific	SP15-100
Slowfade Gold Antifade Reagent	Life technologies	S36942
Critical Commercial Assays/Kits		
NEBNext® Multiplex Small RNA Library Prep Set for Illumina®	NEB	E7300
MinElute Gel Extraction Kit	QIAGEN	28604
Dynabeads Protein A	Life Technologies	10002D
Rhodamine Peanut Agglutinin	Vector laboratories	RL-1072
Deposited Data		
Deep sequencing datasets	This study	GEO accession: GSE119447
All raw imaging data are deposited at Mendeley Data.	This study	https://doi.org/10.17632/4ggdbd7bv9.1
Experimental Models: Organisms/Strains		
Mouse: *Tdrd12 knockout*	(Pandey et al., 2013)	Available with RIKEN Bio Resource Centre; BRC no. RBRC02326
Mouse: *Exd1* knockout	(Yang et al., 2016)	Deposited with EMMA (No. 08303)
Oligonucleotides		
Genotyping primer for *Tdrd12*-forward	(Pandey et al., 2013)	ACTGTTGCTAATGGGAGCTACTGT
Genotyping primer for *Tdrd12*-reverse	(Pandey et al., 2013)	GGGCAGTATCTTTCCTGAGTCATA
Genotyping primer for *Tdrd12*-reverse2	(Pandey et al., 2013)	GCGGAATTCTCTAGAGTCCAGATC
Genotyping primer for *Exd1*-forward	(Yang et al., 2016)	CAGGATTTCTCTGTGTGTTCCTTC
Genotyping primer for *Exd1*-reverse	(Yang et al., 2016)	CTGAAGCCAACAGAGTTTCCCATG
Genotyping primer for *Exd1*-reverse2	(Yang et al., 2016)	CCATCTGCACGAGACTAGTG

(*Continued on next page*)

Continued

REAGENT or RESOURCE	SOURCE	IDENTIFIER
Software and Algorithms		
Sequence read processing and mapping	(Olson et al., 2008)	N/A
R	(R Core Team, 2017)	https://www.r-project.org
Bowtie	(Langmead et al., 2009)	N/A
Other		
MethaPhor agarose	Lonza	50180

CONTACT FOR REAGENT AND RESOURCE SHARING

Further information and requests for resources and reagents should be directed to and will be fulfilled by the Lead Contact Ramesh S. Pillai (ramesh.pillai@unige.ch).

EXPERIMENTAL MODEL AND SUBJECT DETAILS

Animal Work

The use of animals in research at the University of Geneva is regulated by the Animal Welfare Federal Law (LPA 2005), the Animal Welfare Ordinance (OPAn 2008) and the Animal Experimentation Ordinance (OEXA 2010). The Swiss legislation respects the Directive 2010/63/EU. This work was authorized (authorization no. GE/130/17) by the Direction Générale de la Santé and the official ethic committee of the State of Geneva performing a harm-benefit analysis of the project. Animals are treated with respect based on the 3Rs principle in the animal care facility of the University of Geneva. We use the lowest number of animals needed to conduct our specific research project. Discomfort, distress, pain and injury is limited to what is indispensable and anesthesia and analgesia is provided when necessary. Daily care and maintenance are ensured by fully trained and certified staff.

Exd1 and Tdrd12 mutant mice

The mouse knockout mutants for *Tdrd12* (RIKEN Bio Resource Centre; BRC no. RBRC02326) (Pandey et al., 2013) and the *Exd1* (The European Mouse Mutant Archive, EMMA; EM:08303) (Yang et al., 2016) are described. We crossed the fertile homozygous knockout $Exd1^{-/-}$ and heterozygous $Tdrd12^{+/-}$ animals to create fertile $Exd1^{+/-}$; $Tdrd12^{+/-}$ animals. These were further intercrossed to generate animals of the $Exd1^{-/-}$; $Tdrd12^{+/-}$ genotype (referred to as the sensitized *Exd1* mutant), which displays male-specific infertility. For studying the role of EXD1 in MILI slicing-triggered phased piRNA biogenesis, we brought the *Rosa26-pi* artificial piRNA precursor sequence (Yang et al., 2016) into the different *Exd1* genetic backgrounds.

Three different types of control animals were used for the analysis of adult testes phenotypes: fertile $Exd1^{+/-}$;$Tdrd12^{+/-}$, as well as fertile $Exd1^{+/-}$ and C57BL/6 wild-type mice. There were no differences in the testis phenotypes between these three strains, and they were all named as "control." At P24 time point, $Exd1^{+/-}$;$Tdrd12^{+/-}$ was used as a control. Other genotypes analyzed were fertile $Exd1^{-/-}$, infertile $Exd1^{-/-}$;$Tdrd12^{+/-}$ (sensitized *Exd1* mutant) and the infertile $Tdrd12^{-/-}$ mutants.

Genotyping protocols for *Tdrd12* (Pandey et al., 2013) and *Exd1* (Yang et al., 2016) mutants are already described.

METHOD DETAILS

Histology

For histological analysis, mouse testes and epididymis were collected at different time points in Bouin's fixative and incubated 4 to 20 hours at room temperature on multi RS-60 Biosan rotator. Testes were dehydrated 2 × 30 min in 50% ethanol and 2 × 30 min in 70% ethanol before embedding in paraffin. The blocks were cut into 4 μm sections and mounted onto polylysine-coated slides. Paraffin-embedded testis sections were stained with hematoxylin and eosin (HE) or periodic acid-Schiff (PAS) according to standard protocols (Wenda et al., 2017).

Preparation of tissue samples for immunostaining

For paraffin embedding, testes collected from mice at different time points (P24 and P60), and fixed in 4% paraformaldehyde (PFA) in phosphatate-buffered saline (PBS) overnight at room temperature on multi RS-60 Biosan rotator. Testes sections (~4 μM thickness) were prepared using microtome then placed in +37°C over night. Testes samples were dehydrated in a series of ethanol washes as described above, and embedded in paraffin. Paraffin-embedded testis sections were deparaffinzed by incubations: 3 × 5 min in xylene, 2 × 10 min in 100% ethanol, 2 × 10 min in 96% ethanol, 2 × 10 min in 70% ethanol, and then washed in milliQ water 2 × 2 min. Antigen retrieval was performed by incubation in sodium citrate solution (10 mM sodium citrate, 0.05% Tween 20, pH 6.0) for 20 minutes, at 1 atmosphere (atm), at 120°C (achieved in a pressure cooker). Samples were allowed to cool down to

room temperature for at least 2 hours then washed 4 × 3 min in miliQ water and 5 min in PBS before starting with immunofluorescence staining.

For P0 (new-born) testis immunostaining, cryosections (~7 μM thickness) were prepared and dried at room temperature and fixed in cold 4% PFA for 10 min. Samples were washed with PBS and distilled water, then soaked in 10 mM Sodium Citrate buffer (pH 6.0) and boiled in microwave for 20 min. Samples were allowed to cool down at room temperature, treated with 0.3% Triton X-100 for 10 min and washed in PBS before continuing with immunofluorescence staining.

Immunofluorescence analysis

Tissue sections were incubated in blocking solution containing 10% bovine serum albumin (BSA) in PBS with 0.1% Triton X-100 (PBST) for 1 hour at room temperature in a moist incubation chamber. Immunofluorescence staining was performed in blocking solution at 4°C overnight with specific primary antibodies. Tissue sections were washed 3 × 5 min with PBST. AlexaFlour 488/647-conjugated secondary antibodies (Life Technologies) were used in dilution of 1:1000 in blocking solution. Tissue sections were incubated in secondary antibody solution for 1 hour at room temperature in a moist incubation chamber protected from light. Tissue sections were washed 3 × 5 min with PBST, incubated 5 min in DAPI (D9542 Sigma-Aldrich, 5 mg/mL stock) diluted 1:20000 in PBS, washed 5 min in PBS, 5 min in milliQ water and finally mounted with ProLong Diamond Antifade Mountant (P36970, Life Technologies). Stained tissue sections were left for at least 24 hours at room temperature to allow proper solidification of the mounting medium (Wenda et al., 2017).

Imaging

Confocal images were acquired using 3i spinning disk confocal microscope with a 63X Oil objective. Images were processed (background subtraction, contrast and brightness adjustment) with Fiji ImageJ 1.50b. Images for histological analysis were acquired using Leica DMRBE microscope (Carl Zeiss AG) or Panoramic 250 slide scanner (3DHISTECH Ltd) with a 40X objective. Image analysis/seminiferous tubule counting was carried out using Fiji ImageJ cell counter. The percentage of tubules containing specific cell types were calculated and plotted with GraphPad Prism 5.0.

Antibodies

Commercial antibodies

The following antibodies were purchased: anti-MVH (Abcam, ab13840), anti-MIWI (Cell signaling, G82), anti-SCP3 (Santa Cruz Biotechnology, sc-33195), anti-SOX9 (Millipore, AB5535), anti-MILI/PIWIL-2 clone 13E-3 (Reuter et al., 2009) (Millipore, MABE363), anti-γH2AX (Millipore, 05-636), anti-LIN28 (R&D systems, AF3757) to detect mouse proteins. For immunofluorescence studies, the following secondary antibodies were used: Anti-rabbit (Life Technologies; Alexa Fluor 647, A31573) and anti-mouse (Life Technologies; Alexa Fluor 488, A21202), anti-goat (Alexa Fluor 488, A11055). Acrosomes were stained with PNA Rhodamine Peanut Agglutinin (Vector laboratories, RL-1072).

Other antibodies

Antibodies for mouse MILI (mouse monoclonal 13E-3 or rabbit polyclonal FGR9) (Reuter et al., 2009), MIWI2 (rabbit polyclonal FCHE) (Pandey et al., 2013), MIWI (rabbit polyclonal 3BW8 and BTO) (Reuter et al., 2011), and mouse LINE1 ORF1p (rabbit polyclonal GJAE) are described previously (Wenda et al., 2017).

Immunoprecipitation of PIWI proteins and sequencing libraries

Immunoprecipitation of MILI and MIWI2 complexes from P0 (new-born pups) testes were carried out as previously described (Wenda et al., 2017). While MILI libraries were made directly from the immunoprecipitated RNAs, MIWI2-associated small RNAs (24-30nts) were purified from denaturing urea gel for library preparation. Deep sequencing libraries of P0 and P12-P14 testicular total small RNAs (19-40 nt) were prepared as described (Yang et al., 2016). Library preparation of immunoprecipitated RNAs and sequencing were as previously described (Wenda et al., 2017). All datasets used in this study are listed in Table S1.

QUANTIFICATION AND STATISTICAL ANALYSIS

Analysis of reads originating from artificial piRNA precursor (Rosa26-pi)

The analysis was done as previously (Wenda et al., 2017). Briefly, reads of at least 15 nucleotides were aligned to the *Rosa26-pi* sequence using bowtie (Langmead et al., 2009) allowing no mismatches. The abundance of reporter-derived piRNAs (24-30 nt reads) and 16-mer by-products was compared in between individual samples (Figure S1B,D). To investigate the distribution, we mapped the 5′ and 3′ ends of piRNAs and 3′ ends of 16-mers along the reporter and calculated their distance from the closest site targeted by MILI piRNA (i.e., 5′ end of targeting piRNA) (Figure S1C). Slicer-triggered piRNAs and 16-mer by-products generated by slicing activity of MILI, were detected in the *Exd1*$^{-/-}$ mutant.

Analysis of total small RNA libraries

Reads were sorted into individual libraries based on the barcodes, the 3′ adaptor sequences were removed and mapped to the mouse genome (mm10). The software used for processing the data (genomic coordinates etc) from the raw data files are in-house tools developed by the Sachidanandam lab (Olson et al., 2008). Only reads perfectly matching the genome, and of minimum 15 nt in

length, were kept for further analysis. The reads from total small RNA libraries were divided into two groups based on whether they match to single or multiple locations in the genome. Comparison of read length distribution between P0 *Tdrd12*$^{+/-}$;*Exd*$^{-/-}$ and *Tdrd12*$^{+/-}$;*Exd1*$^{+/-}$ showed apparent enrichment of multi-mapped reads of 30-34nt in *Tdrd12*$^{+/-}$;*Exd1*$^{-/-}$ and decrease of piRNAs (Figure 3A,B; Figure S3A,B). Classification of piRNA reads (25-29nt) based on genome annotation showed that mainly repeat antisense reads are affected (Figure 3C-E). But the decrease was apparent also for repeat sense piRNAs (Figure S3C,D).

To visualize the difference in LINE1 piRNA abundance we mapped the 5′ ends of genome mapped 25-29 nt piRNAs to L1 repeat consensus sequence allowing at maximum of 3 mismatches (Figure 3F). Read counts were normalized to library sizes and divided by counts of mapped genomic sites. These reads were also used for the ping-pong analysis (Figure 3H), where the product of the piRNA counts was used to calculate the score for the 5′ end distance Δ: score(Δ) = ΣM(i)*N(i+Δ) where M(i) is the count of produced piRNAs (in rpm) with 5′ end on the plus strand at a particular position i and N(i+Δ) is the count of piRNAs which have their 5′ end position at minus strand at i + Δ. The ping-pong signature refers to the peak at distance 9, which corresponds to 10 nt overlap of piRNA 5′ ends. The signature was reduced in both *Tdrd12*$^{+/+}$;*Exd1*$^{-/-}$ and the sensitized *Tdrd12*$^{+/-}$;*Exd1*$^{-/-}$ genotypes to a similar extent.

Classification of 30-34 nt reads based on genome annotation showed that the reads almost exclusively originate from tRNAs (Figure S3E-G) and therefore correspond to tRNA fragments (tRFs). To find out which part of tRNAs generate the tRFs, FASTA sequences of tRNAs were downloaded from gtRNAdb (http://gtrnadb.ucsc.edu) and the individual reads were re-aligned to these tRNA sequences by bowtie (Langmead et al., 2009) allowing no mismatches. Abundance of reads originating from tRNAs was plotted separately for 25-29nt reads (piRNAs) and 30-34nt reads (tRFs) as percentage of all sequenced reads (Figure S3H). Read counts of reads aligning to multiple tRNAs were divided by number of tRNAs they aligned to and the 5′, 3′ and whole read coverage was calculated separately for 25-29nt reads (piRNAs) and 30-34nt reads (tRFs) for individual tRNAs. Meta-coverages were then calculated and plotted for 5′ portion of tRNAs (nucleotide positions:1-51) (Figure S3I). For two tRNAs producing the most of tRFs, the 3′ ends of tRFs were depicted on the secondary structure of tRNAs which demonstrated that the cleavages generating the 3′ ends occur preferentially at the start of the anticodon loop (Figure S3J).

In P10 total small RNA libraries, the read length profiles were highly similar between the genotypes (Figure S5A) and the overall levels of piRNAs and also longer reads were not different (Figure S5B). Only LINE sense piRNAs were elevated in *Tdrd12*$^{+/-}$;*Exd1*$^{-/-}$ (Figure S5C). Same increase was apparent for piRNAs which mapped to the L1 repeat consensus with maximum 3 mismatches (Figure S5D,E).

Analysis of small RNA libraries from MILI and MIWI2 complexes

Reads were sorted into individual libraries based on the barcodes, the 3′ adaptor sequences were removed and mapped to the mouse genome (mm10). The software used for processing the data (genomic coordinates etc) from the raw data files are in-house tools developed by the Sachidanandam lab (Olson et al., 2008). Length distribution of the reads was plotted which showed the absence of 30-34 nt reads (tRFs) in both MILI and MIWI2 libraries (Figure 4B), indicating that the tRF reads present in the total small RNA libraries are not loaded into PIWI proteins. Therefore, further analysis focused only on piRNAs (24-31 nt). Genome annotation of piRNAs showed that piRNAs targeting LINE elements are underrepresented in MIWI2 libraries of both *Tdrd12*$^{+/+}$;*Exd1*$^{-/-}$ and the sensitized *Tdrd12*$^{+/-}$;*Exd1*$^{-/-}$ mutants, with a stronger decrease in the latter (Figure 4C,D). Similar effect was observed when mapping the piRNAs along the L1 consensus sequence (Figure 4E). Both *Tdrd12*$^{+/+}$;*Exd1*$^{-/-}$ and *Tdrd12*$^{+/-}$;*Exd1*$^{-/-}$ displayed reduced ping-pong signature (peak at distance 9) in between MILI and MIWI2 L1 piRNAs (Figure S4E).

DATA AND SOFTWARE AVAILABILITY

The accession number for the deep sequencing data reported in this study is GEO: GSE119447. All raw imaging data and gel pictures are deposited with Mendeley Data and is available here: https://doi.org/10.17632/4ggdbd7bv9.1